Influence of Cobalt Substitution in $LaMnO_3$ on Catalytic Propylene Oxidation

Teotone Inas Mariano Vaz[1*], Sridhar Maruti Gurav[2], and Arun Vithal Salker[3]

[1]*Department of Chemistry, St. Xavier's College, Mapusa Goa, India*

[2]*Government College of Arts, Science and Commerce, Quepem, Goa 40375, India*

[3]*School of Chemistry, Goa University, Goa 403206, India*

* ***Corresponding author:***

email: teovaz18@gmail.com

Received: May 8, 2021
Accepted: August 19, 2021

DOI: 10.22146/ijc.65766

Abstract: *Perovskite-type structures $LaBO_3$ with the compositions of $LaMn_{1-x}Co_xO_3$ (x = 0.0, 0.3, 0.5, 0.7, and 1.0) were synthesized at 800 °C by a modified co-precipitation precursor technique for total oxidation of propylene, as a model test of the hydrocarbon oxidation reaction. Details concerning the evolution of the crystal structure, morphology, and crystallite size were performed by X-ray diffraction (XRD), Thermo Gravimetry Analysis (TGA)/Differential Scanning Calorimetry (DSC), Fourier Transform Infra-Red (FTIR), Atomic Absorption Spectroscopy (AAS), Scanning Electron Microscopy (SEM), and Electron Spin Resonance (ESR) techniques. All compositions were identified to be single-phase and are indexed to rhombohedral structures. TG/DSC technique evidenced a temperature of 330 °C needed for the precursor as the start point and 800 °C completion for perovskite phase formation. Slight distortion in XRD diffraction peaks was observed on substituting manganese with cobalt in B-site, and new peaks emerged. An attempt has been made to understand the effect of the B-site substitution of Co^{3+} ions in the lattice of $LaMnO_3$ and their influence on catalytic total propylene oxidation efficiency. These compounds show a considerable increase in the activity of propylene oxidation to carbon dioxide and water and could be explored for hydrocarbon pollution control.*

Keywords: *rare earth perovskites; co-precipitation; catalytic oxidation; propylene*

■ INTRODUCTION

The perovskite-type $LaBO_3$ structures based on transition metal ions have been the object of intense scientific research due to their fascinating physical properties. They exhibit an array of applications in microelectronics, supercapacitor electrodes, micro-actuators in MEMS, thermoelectric energy harvesters, magneto electronics, sensors, magnetic memory devices, solar cells, and catalysts [1-6]. $LaBO_3$ (B = Mn, Ni, Co) has been studied as prospective materials for protective coating owing to their structural and chemical stability at high temperatures and high electrical conductivity in solid oxide fuel cells. Their unique crystal structure and physicochemical properties indicate their great potential as supercapacitor materials for fast energy storage applications [7]. The La ions support the framework, stabilizes the system, and hence the size of these ions defines the octahedral structural transformations, which in turn decides the physical properties, governs the electronic state and the phase transition. A perovskite-type mixed metal oxide with ABO_3 structure, wherein the cation with larger radius is coordinated to 12 oxygen atoms and occupy A- and B- sites. A and O form the closest cubic packing, and B occupy octahedral voids in the lattice. Incorporated ions of various sizes and charges show great structure flexibility with the substitution in A- and/or B- site, leading to fascinating large-scale applications. The ions substitution, leading to deviation from ideal stoichiometry, resulted in altering the electronic properties. Meanwhile, the robust structure of these oxides can accommodate a large number of metals to improve the quality of materials, offering high possibilities space for catalysis [8]. Catalytic combustion provides one of the most effective means of controlling automobile pollution. Compared with presently in use

noble metal, other metal oxide catalysts offer sufficient activity and thermal stability as oxidation catalysts, having advantages of economic viability and potential usage in the energy-generating systems and a promising candidate for an auto exhaust catalyst [9].

In general, a large number of elements can be obtained as ideal cubic or modified perovskites structures depending upon their tolerance factor. The ideal structure is most successful for a tolerance factor close to 1 and suitable temperatures. In other conditions, preferred distortions orthorhombic, rhombohedral, and to a lesser extent, tetragonal, mono, or triclinic perovskites will appear [9]. It has been known that a particular synthetic route influences the physical changes in the volume and surface properties of the material, for example, its structure, morphology, porosity, and particle size [8,10]. Novel synthesis techniques have been developed to prepare comparatively pure form perovskite materials either by modified conventional ceramic, co-precipitation, sol-gel, hydrothermal, auto-combustion, and other modern techniques like aerosol, pulse laser, spray pyrolysis, and solution-polymerization techniques [1-3,8,11]. Even today, the modified co-precipitation precursor is a straightforward method to obtain these nanocrystalline range materials in the pure phase.

Metal oxides catalyze the oxidation of propylene with oxygen giving rise either to partial (selective) or total oxidation to CO_2. The total oxidation of propylene to reduce air pollutants is a critical consideration in automobile and industrial pollution control. Several investigators have studied the solid-state and the catalytic activity of propylene oxidation over several $LaBO_3$ compounds. Their studies have shown that the non-noble metal-containing $LaBO_3$ catalysts are chemically active species for total hydrocarbon oxidation [2,10,12-14]. In the present investigation, an attempt is made to understand the effect of B-site substitution of Mn atom by Co in the lattice of $LaMnO_3$, its influence, and the comparative catalytic activity of the progressively substituted $LaMnO_3$ with various cationic compositions prepared by co-precipitation precursor technique, in the total oxidation of propylene and their correlation with the structural properties.

■ EXPERIMENTAL SECTION

Materials

Analytical grade pure reagents $La(NO_3)_3{\cdot}6H_2O$, $Mn(NO_3)_3{\cdot}6H_2O$, $Co(NO_3)_3{\cdot}6H_2O$, and 6% H_2O_2 were used to synthesize the desired perovskite nanomaterials.

Instrumentation

TGA/DSC curves were carried out on a representative hydroxide precursor, using NETZSCH - Garetebau GmbH Thermal Analyzer to determine the required temperature to complete the perovskite phase. The system compositions were characterized by X-ray powder diffraction technique with Rigaku Miniflex tabletop instruments, using Cu-Ka, filtered through Ni absorber. FTIR spectra were recorded on a Shimadzu FTIR instrument (model 8101A). The sodium contamination in the perovskites prepared by the co-precipitation method using sodium hydroxide was found by employing atomic absorption spectroscopy. The total BET surface areas were measured using the BET nitrogen adsorption method (QUANTACHROME NOVA 1200 version 3.70).

The physical structure of catalysts, compositional analysis, and surface morphology observations was determined by scanning electron microscopy by a ZEISS instrument. ESR study was carried out for the perovskites containing paramagnetic species and to identify the catalytically active species for the reaction. The ESR spectra were recorded at the X- band on a Varian E-112 spectrophotometer at liquid nitrogen temperature. The sample was mounted on a quartz tube, and Tetracyanoethylene was used as a field calibrant taking its g-value as 2.00277. The saturation magnetization was studied using a high field hysteresis loop tracer, considering the hysteresis behavior on a selected magnetic sample. The saturation magnetization values, σs in emu/g, of some magnetic perovskite samples were measured.

Total propylene oxidation was studied as a model test reaction using oxygen in nitrogen with a continuous flow, fixed bed quartz reactor by placing 1 g of powdered catalyst between glass wool plugs. The catalyst activity

was determined using a feed gas composition of 5% propylene, 10% O_2 in nitrogen. The individual gas flow rates were controlled using flow meters and precision needle valves. The feed gases and the products were analyzed employing an online gas chromatograph with a molecular sieve 13X and Porapak N columns. H_2 was used as a carrier gas. The propylene, oxygen, and nitrogen gases were used from pure commercial cylinders, further purified through alkali and molecular sieve traps [15].

Procedure

The perovskite-type compositions of $LaMn_{1-x}Co_xO_3$ were synthesized by the hydroxide co-precipitation precursor technique at 800 °C, as discussed elsewhere [15]. In brief, the procedure involved is as follows. All calculations were performed for 10 g of the desired product. The respective quantities of hydrated salts $La(NO_3)_3$, Mn/Co nitrates (AR) were weighed in g and dissolved together in 100 mL of distilled water. Aqueous solutions were mixed on a magnetic stirrer and slowly precipitated, adding approximately 50 mL of equimolar sodium hydroxide solution. The precipitate obtained was digested for 15 min, checked for complete precipitation, and the resultant precipitate mixture was subjected to oxidation using 10 mL of 6% H_2O_2 solution. It was allowed to set overnight. The hydroxide precursor precipitate was then washed, filtered, and dried in an oven at 150 °C. A small portion of it was preserved for TG/DSC analysis. The dried precipitate was homogenized well in an agate mortar and further heated at 300, 600, and finally at 800 °C in the air for a total time of 10–12 h. The furnace-cooled compositions were stored in air-tight containers for characterization and further propylene oxidation.

■ RESULTS AND DISCUSSION

TG/DSC Analysis

TG/DSC curves were recorded to study the behavior of weight loss of the hydroxide precursor. Fig. 1 displays a typical TG-DSC curve of selected $LaMn(OH)_6{\cdot}xH_2O$ precursor from r.t. to 900 °C. The powdered form of a precursor (approx. 20 mg) was placed in an alumina crucible, covered with a lid, and continuously weighed as

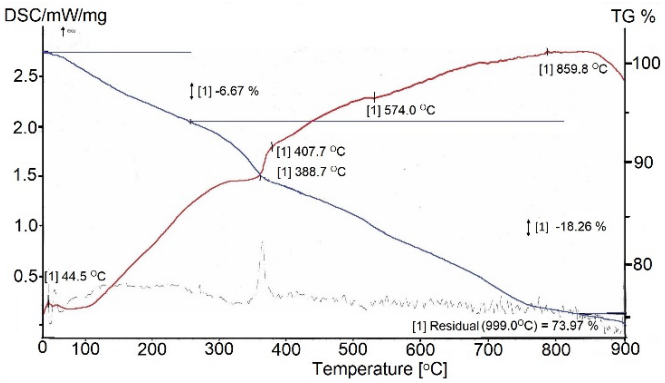

Fig 1. TG/DSC curves for $LaMn(OH)_6.xH_2O$ precursor

it is heated at a constant linear rate of 10 °C/min. An endothermic event around 80 °C was the usual loss of moisture from the precursor, and a negligible mass loss in the TG curve was observed. The weight loss of 6.67% between r.t. to 275 °C due to the loss of moisture. The decomposition of $LaMn(OH)_6$ was observed in the range of 275 to 408 °C. After that, the initiation of a solid-state diffusion process begins. Further, the decomposition of hydroxides and observed linear weight loss is due to initiation of solid-state diffusion with the together weight loss of 18.26% and perovskite phase formation between 400–800 °C in agreement with the literature [16].

XRD Analysis

The phase composition and the crystal structure of the prepared perovskite materials were characterized using X-ray powder diffractograms. Fig. 2 shows XRD patterns for $LaMn_{1-x}Co_xO_3$ perovskite materials, after thermal treatment in stages and finally calcined at 800 °C. The d_{hkl} and 2θ values obtained were compared with those reported in the literature (JCPDS data file) and found in good agreement. Since the d_{hkl} value of the intermediate compositions is not reported, the values were compared with the end compositions. Our results of X-ray analysis revealed that the end compositions $LaMnO_3$ and $LaCoO_3$ could be clearly indexed to rhombohedral structure perovskites, with space group *R-3c*, following the JCPDS file 25-1060 and 48-0123, respectively. The general appearance of the diffractograms remains uniform, as all the compositions belong to the same crystal structure family. It may be

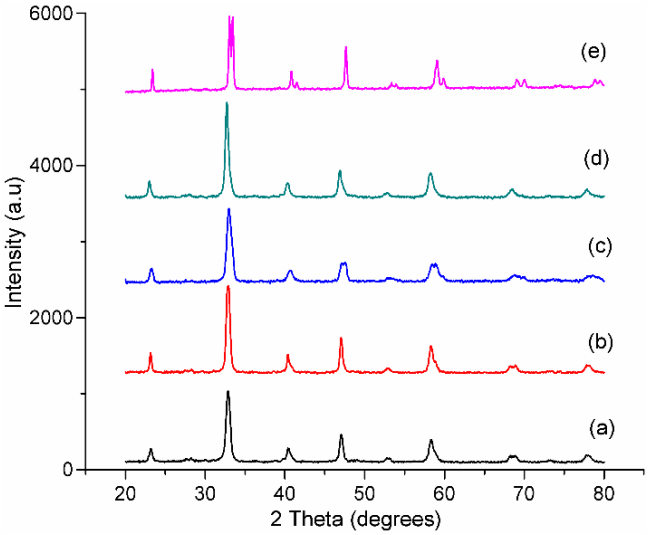

Fig 2. XRD patterns of (a) $LaMnO_3$, (b) $LaMn_{0.7}Co_{0.3}O_3$, (c) $LaMn_{0.5}Co_{0.5}O_3$, (d) $LaMn_{0.3}Co_{0.7}O_3$, and (e) $LaCoO_3$ nanoperovskites

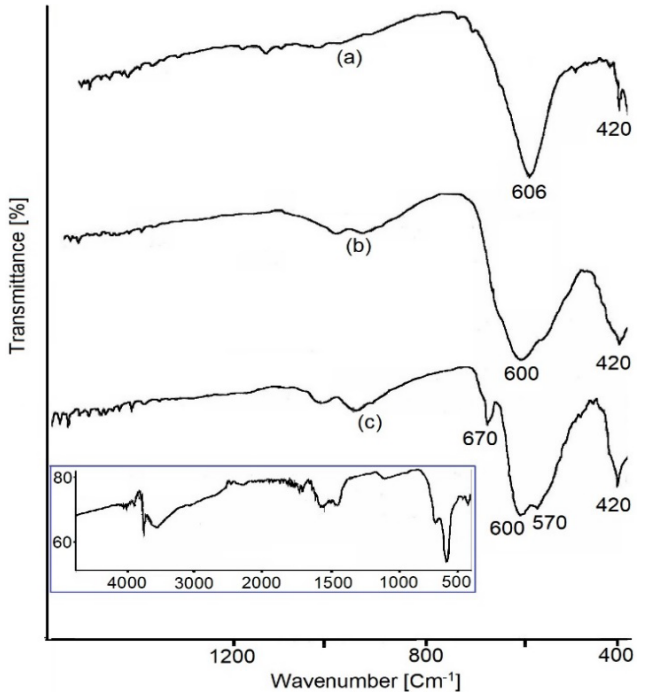

Fig 3. FTIR spectra (a) $LaMnO_3$, (b) $LaMn_{0.5}Co_{0.5}O_3$, and (c) $LaCoO_3$ nanoperovskites. Inset: Spectra of $LaCo(OH)_6.H_2O$ precursor

interesting that the diffraction angles remain the same for all intermediates, with only minor changes in the intensity due to the Mn/Co ratio.

Moreover, it can be seen that the main characteristic peak at around 32.7° moves slightly to a lower angle with the increase in Co concentration. The observed characteristic splitting in the diffraction peaks is evidence of the rhombohedral distortion of the perovskite structure. The crystallite particle sizes calculated from the four intense diffraction peaks data using Debye Scherrer's formula were in the range of 11.99–20.70 nm, confirming their nanocrystalline nature.

AAS and FTIR Analysis

The sodium contamination was estimated using an AAS and found to be 0.2 to 0.4% by weight. Surface areas obtained by the BET nitrogen adsorption method were found to be in the range of 5.4–12.6 m^2/g for these nanoperovskites, highest for $LaMn_{0.5}Co_{0.5}O_3$ composition. The perovskite structure is characterized using IR spectra in the region of 1000 to 300 cm^{-1} [17]. Fig. 3 illustrates the characteristic absorption bands for selected The IR spectra showed that the compound has tensile energy bands in the B–O–B bonds related to the MO_6 (B = Mn or Co) Octahedron, which are attributed to the characteristic stretching vibration of the M–O bond frequencies of perovskite structure, i.e., the B–O–B bond angles. The comparatively sharper lower absorption frequencies observed at 600 and 420 cm^{-1} in $LaMnO_3$ are assigned to a deformation mode of MnO_6 octahedron. It may be noted that with the substitution of Co^{3+} in $LaMnO_3$ lattice, both characteristic strong absorption perovskite peaks get gradually broadened. Further, the peak at 600 cm^{-1} gets shouldered for x = 0.5 and 0.7 compositions. The FTIR spectra for x = 0.3, 0.5, and 0.7 show similar patterns, whereas, for $LaCoO_3$, distorted shouldered peaks at 600 cm^{-1} and 570 cm^{-1} were observed, which indicate slight structural symmetry change in agreement with the literature [17]. Inset shows absorption spectra of a selected precursor.

SEM and Surface Area Analysis

Fig. 4 shows representative SEM images of $LaMn_{1-x}Co_xO_3$ nanoperovskite materials with 80.00 kV magnifications. In all the images, particles with semi to spherical shapes can be observed. The micrograph of

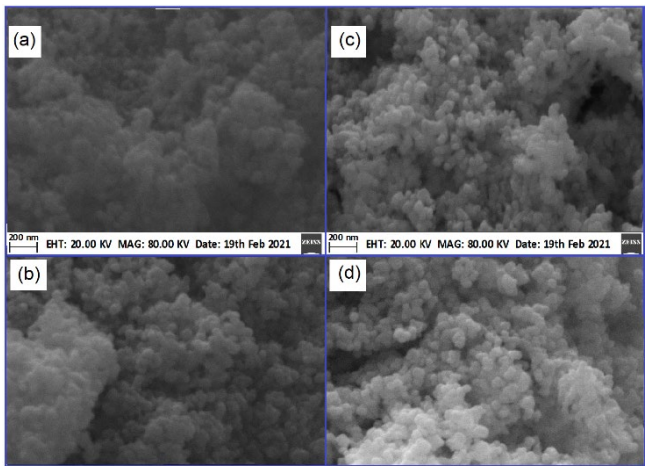

Fig 4. SEM image of (a) $LaMnO_3$, (b) $LaMn_{0.5}Co_{0.5}O_3$, (c) $LaMn_{0.3}Co_{0.7}O_3$, and (d) $LaCoO_3$ polycrystalline nanoparticles

$LaMnO_3$ in Fig. 4(a), no clear particle structure, but granular spherical nanoparticles agglomeration was observed. In Fig. 4(b), the spherical particles have become distinct for x = 0.5 and further clarity in the particle shape is distinct in Fig. 4(c) for x = 0.7. For $LaCoO_3$, as observed in Fig. 4(d), a clear spherical-shaped structure is prominent. Significant morphological changes are observed when B-site Mn is substituted with more oxyphilic Co atoms, promoting better spherical-shaped particles having higher porosity. Overall, the morphology results from the agglomeration of very small polycrystalline particles in the nano range. In addition, surface areas obtained by the BET nitrogen adsorption method were in the range of 5.4–12.6 m^2 for these compositions.

ESR Analysis

All the nanocatalyst materials showed Lorentzian-shaped ESR lines. It is clearly visible that the g-value of the $LaMn_{1-x}Co_xO_3$ nanosystem is found to increase with increasing 'x' value. Fig. 5 shows ESR spectra of different perovskites at liquid N_2 temperature. No signal at r.t. and a very weak ESR signal with broad line width was observed only at liquid nitrogen(N_2), indicating that Mn^{3+}, Mn^{4+}, and Co^{3+} ions are ESR inactive. For heavier atoms like La^{3+}, the spin-orbit coupling is strongly coupled to lattice vibrations and spin relaxation time. Therefore, it is very small at high temperatures, so ESR spectra are too broad to

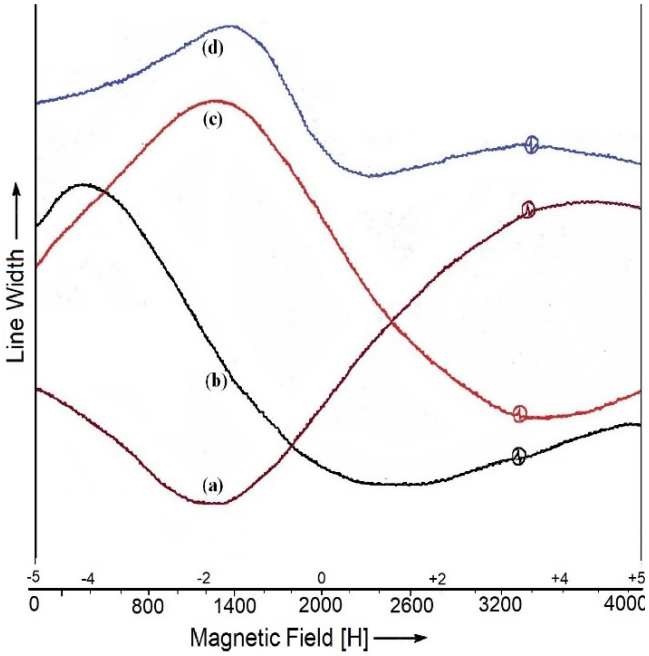

Fig 5. ESR plots of a) $LaMnO_3$ b) $LaMn_{0.7}Co_{03}O_3$, $LaMn_{0.5}Co_{0.5}O_3$, and d) $LaCoO_3$

be detected even at r.t. The observed g-values were 2.9, 4.5, and 3.0 for x = 0, 0.3, and 0.5 compositions respectively. For $LaCoO_3$, the g-values of 3.7 were observed in agreement with the literature [18].

The temperature dependence of propylene oxidation studies on different compositions of the $LaMn_{1-x}Co_xO_3$ system is shown in Fig. 6. The results showed some interesting activity trends. The incorporation of Co^{3+} ions in the $LaMnO_3$ lattice showed a decline in the catalytic activity, except for x = 0.7. The catalytic activity efficiency is in the order of x = 0.3 > 0.0 > 0.5 > 1.0 > 0.7. The induction temperature for all the catalyst nanomaterials was uniformly at 100 °C. At 200 °C all catalysts showed 10 to 30% oxidation and at 400 °C, x = 0.3 composition showed around 70% and x = 0.7 showed 40% oxidation efficiency. At 450 °C, the catalytic trend continues, and the first three catalysts show an efficiency of 75–80% total oxidation and the highest for $LaMn_{0.7}Co_{0.3}O_3$. It may also be noted that the incorporation of Co^{3+} ions in the lattice showed a significant rise in the catalytic activity throughout. $LaMn_{0.3}Co_{0.7}O_3$ nanocatalyst showed comparatively low oxidation capacity despite having a comparatively higher specific surface area in the system.

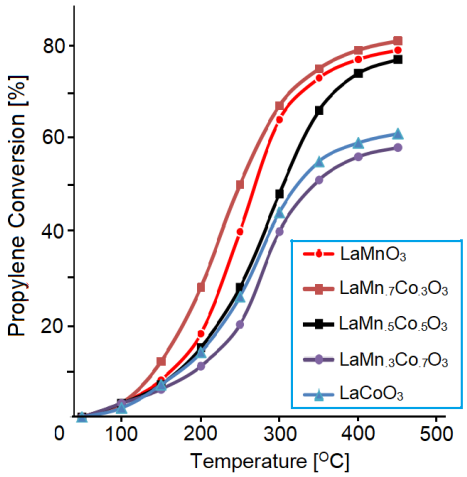

Fig 6. Catalytic propylene oxidation on $LaMn_{1-x}Co_xO_3$ system

The mechanism of heterogeneous catalytic oxidation essentially involves interaction between a hydrocarbon molecule and surface-active oxygen. In $LaBO_3$ perovskites, La ions are essentially inactive in catalysis catalytically inactive, and B-site active transition metal ions are placed at relatively large distances from each other are excellent catalytic models for the study of interactions of propylene and O_2 on a single surface site. Since in our study, A-site La^{3+} ions, being present in the same amount in all compositions, the observed differences in a catalytic activity need to be explained for increasing Co^{3+} ions substitution, replacing Mn^{3+} ions in B-site and its effect on $LaMnO_3$ crystal structure. The active transition metal B ions are situated in the center of an octahedron, whose vertices are occupied by O ions. The B–O bond strength differs for each member of the transition series, depending upon their tolerance factor [19]. Therefore, under the condition of adsorption and catalysis, different surface defect concentrations and nature may be produced in each of these oxides. The change in crystal field stabilization energy is due to the change in the coordination number of B^{3+} ions on adsorption of oxygen and their experimental profiles of adsorption and catalysis [2,14,20]. Thus, the relationship between the local symmetry of surface cations, adsorption, and catalysis, shows the importance of localized interactions of these surface processes.

On the other hand, the observed relation between the catalytic activity for the total oxidation and the O_2 adsorption shows that the adsorbed oxygen (not the lattice oxygen) plays an important role in the catalytic reaction. The chemisorption of oxygen and the total oxidation of propylene on $LaBO_3$ perovskites are interrelated. The catalytic activity increases in the same order as the adsorption of oxygen on a clean surface. In $LaMnO_3$ and $LaCoO_3$ perovskite materials, the Mn^{3+} and Co^{3+} ions are positioned in the octahedral environment, whose vertices are occupied by O atoms. The metal-oxygen bond strength is different for Mn–O and Co–O bonds, leading to varying surface defect concentrations. The observed catalytic results are discussed within the framework of local symmetry of surface cations, its influence on catalysis, and the importance of localized interactions in propylene oxidation. Though there is no direct relation observed between the catalytic activity trend and specific surface area of the materials under study, the specific surface area of $LaMnO_3$ is almost double that for $LaCoO_3$, which may have considerably increased in the oxygen adsorption on the surface of catalytic materials. The adsorbed oxygen plays an important role in the catalytic reaction, thus slightly increasing the catalytic activity of $LaMnO_3$ material. For the total hydrocarbon oxidation, the parallelism observed for the catalytic activity and oxygen adsorption, i.e., the suitable adsorbents exhibiting higher catalytic activity, shows that the adsorbed oxygen plays an important role. This fact indicates that the total oxidation of propylene occurs through the suprafacial catalysis mechanism. The catalyst provides orbitals of appropriate energy and symmetry for the bond formation with the reactant and intermediate. In this mechanism, the adsorbed oxygen and not the lattice oxygen participate in the catalytic oxidation reaction.

Further, the oxygen adsorption and the total oxidation of propylene on $LaCoO_3$ are attributed to propylene's activation energy and the bond strength, with the adsorbent surface greatly influencing the catalytic action for oxidation by these perovskite materials [2]. The observed trend of catalytic activity was

similar to the similar work of total propane oxidation published in the very recent work [12], where authors have focused on the reaction kinetics of slightly different compositions $LaMn_{1-x}Co_xO_3$ system. Unfortunately, to our knowledge, there are very few literature reports available for the total hydrocarbon oxidation studies and their correlation with the structure of this class of $LaMn_{1-x}Co_xO_3$ material systems.

■ CONCLUSION

Crystalline $LaMn_{1-x}Co_xO_3$ system perovskite nanomaterials were successfully synthesized at a reasonably low temperature of 800 °C. The phase purity was confirmed with XRD and found to crystallized in rhombohedral perovskite structures. The specific surface area was in the range of 5.4 to 12.6 m^2/g. These compounds are ESR inactive at room temperature but showed broad peaks at liquid nitrogen due to spin-orbit coupling. La^{3+}, Mn^{3+}, and Co^{3+} ions are ESR inactive. SEM micrographs reveal the prominent spherical-shaped agglomerates and Co concentration, promoting very small polycrystalline particles in the nano range. These materials were efficient for total propylene oxidation for emission control of hydrocarbon compounds as pollutants. $LaMnO_3$ shows catalytic propylene oxidation as high as 80% at 400 °C, whereas $LaCoO_3$ shows 60% and may correlate with its specific surface area. The observed trend can be associated with adsorbed oxygen on the catalyst surface, exhibiting higher catalytic activity, and occurs through the suprafacial catalysis mechanism. These nanomaterials show a considerable increase in propylene oxidation that could be explored for hydrocarbon pollution control.

■ REFERENCES

[1] Chávez-Guerrero, L., Medina-Lott, B., Cienfugos, R.F., Garza-Navarro, M.A., Vannier, R.N., Ringuedé, A., Hinojosa, M., and Cassir, M., 2015, Synthesis and characterization of $LaNi_xCo_{1-x}O_3$: Role of microstructure on magnetic properties, *J. Rare Earths*, 33 (3), 277–281.

[2] Peña, M.A., and Fierro, J.L.G., 2001, Chemical structures and performance of perovskite oxides, *Chem. Rev.*, 101 (7), 1981–2018.

[3] Assirey, E.A.R., 2019, Perovskite synthesis, properties and their related biochemical and industrial application, *Saudi Pharm. J.,* 27 (6), 817–829.

[4] Shah, A.A., Ahmad, S., and Azam, A., 2020, Investigation of structural, optical, dielectric and magnetic properties of $LaNiO_3$ and $LaNi_{1-x}M_xO_3$ (M = Fe, Cr & Co; x = 5%) nanoparticles, *J. Magn. Magn. Mater.*, 494, 165812.

[5] Ma, P., Lei, N., Yu, B., Liu, Y., Jiang, G., Dai, J., Li, S., and Lu, Q., 2019, Flexible supercapacitor electrodes based on carbon cloth-supported $LaMnO_3$/MnO nano-arrays by one-step electrodeposition, *Nanomaterials*, 9, 1676.

[6] Kun, R., Populoh, S., Karvonen, L., Gumbert, J., Weidenkaff, A., and Busse, M., 2013, Structural and thermoelectric characterization of Ba substituted $LaCoO_3$ perovskite-type materials obtained by polymerized gel combustion method, *J. Alloys Compd.*, 579, 147–155.

[7] Park, B.K., Song, R.H., Lee, S.B., Lim, T.H., Park, S.J., Park, C.O., and Lee, J.W., 2016, Facile synthesis of Ca-doped $LaCoO_3$ perovskite via chemically assisted electrodeposition as a protective film on solid oxide fuel cell interconnects, *J. Electrochem. Soc.*, 163, F1066.

[8] Carneiro, J.S.A., Williams, J., Gryko, A., Herrera, L.P., and Nikolla, E., 2020, Embracing the complexity of catalytic structures: A viewpoint on the synthesis of nonstoichiometric mixed metal oxides for catalysis, *ACS Catal.*, 10 (1), 516–527.

[9] Silva, P.R.N., and Soares, A.B., 2009, Lanthanum based high surface area perovskite-type oxide and application in CO and propane combustion, *Ecletica Quim. J.*, 34 (1), 31–38.

[10] Gildo Ortiz, L., Guillén Bonilla, H., Santoyo Salazar, J., Olvera, M.L., Karthik, T.V.K., Campos González, E., and Reyes Gómez, J., 2014, Low temperature synthesis and gas sensitivity of perovskite-type $LaCoO_3$ nanoparticles, *J. Nanomater.*, 2014, 164380.

[11] Athayde, D.D., Souza, D.F., Silva, A.M.A., Vasconcelos, D., Nunes E.H.M., Diniz da Costa,

J.C., and Vasconcelos, W.L., 2016, Review of perovskite ceramic synthesis and membrane preparation methods, *Ceram. Int.*, 42 (6), 6555–6571.

[12] Zhu, W., Chen, X., Liu, Z., and Liang, C., 2020, Insight into the effect of cobalt substitution on the catalytic performance of $LaMnO_3$ perovskites for total oxidation of propane, *J. Phys. Chem. C*, 124 (27), 14646–14657.

[13] Li, X., Chen, D., Li, N., Xu, Q., Li, H., He, J., and Lu, J., 2021, Highly efficient Pd catalysts loaded on $La_{1-x}Sr_xMnO_3$ perovskite nanotube support for low-temperature toluene oxidation, *J. Alloys Compd.*, 871, 159575.

[14] Liu, Z., Li, Z., Chu, X., Shao, Y., Li, K., Chen, X., Liu, H., Chen J., and Li, J., 2020, B-sites modification of $LaMn_{0.9}Co_{0.1}O_3$ perovskite using selective dissolution method in C_3H_6 oxidation, *Catal. Sci. Technol.*, 10 (19), 6464–6467.

[15] Salker, A.V., and Vaz, T., 2004, Electrical, magnetic and catalytic oxidation studies on $LaMn_{1-x}Co_xO_3$ system, *Indian J. Chem.*, 43A (4), 710–714.

[16] Tepech-Carrillo, I., Escobedo-Morales, A., Pérez-Centeno, A., Chigo-Anota, E., Sánchez-Ramírez, J.F., López-Apreza, E., and Gutiérrez-Gutiérrez, J., 2016, Preparation of nanosized $LaCoO_3$ through calcination of a hydrothermally synthesized precursor, *J. Nanomater.*, 2016, 6917950.

[17] Sudheendra, L., Seikh, M.M., Raju, A.R., and Narayana, C., 2001, An infrared spectroscopic study of the low-spin to intermediate-spin state ($^1A_1$–$^3T_1$) transition in rare earth cobaltates, $LnCoO_3$ (Ln = La, Pr and Nd), *Chem. Phys. Lett.*, 340 (3-4), 275–281.

[18] Oliva, C., and Forni, L., 2000, EPR and XRD as probes for activity and durability of $LaMnO_3$ perovskite-like catalysts, *Catal. Commun.*, 1 (1-4), 5–8.

[19] Özbay, N., and Şahin, R.Z.Y., 2017, Preparation and characterization of $LaMnO_3$ and $LaNiO_3$ perovskite type oxides by the hydrothermal synthesis method, *AIP Conf. Proc.*, 1809, 020040.

[20] Sui, Z.J., Vradman, L., Reizner, I., Landau, M.V., and Herskowitz, M., 2011, Effect of preparation method and particle size on $LaMnO_3$ performance in butane oxidation, *Catal. Commun.*, 12 (15), 1437–1441.